

Patient-Specific Echo-Based Left Ventricle Models for Active Contraction and Relaxation Using Different Zero-Load Diastole and Systole Geometries

* Longling Fan¹, Jing Yao², Chun Yang³, Di Xu², † Dalin Tang^{1,4}

¹School of Mathematics, Southeast University, Nanjing, 210096, China.

²Department of Cardiology, Nanjing Medical University, Nanjing 210029, China.

³China Information Tech. Designing & Consulting Institute Co., Ltd., Beijing, 100048, China.

⁴Mathematical Sciences Department, Worcester Polytechnic Institute, Worcester, MA 01609.

*Presenting author: fan_longling2008@126.com

†Corresponding authors. Dalin Tang, email: dtang@wpi.edu

Abstract

A new modeling approach using two different zero-load geometries (diastole and systole) was introduced to properly model active contraction and relaxation for more accurate stress/strain calculations. Ventricle diastole and systole material parameter values were also determined based on in vivo data. Echo image data were acquired from 10 healthy volunteers at the First Affiliated Hospital of Nanjing Medical University with consent obtained. Echo-based computational two-layer left ventricle (LV) models using one zero-load geometry (1G) and two zero-load geometries (2G) were constructed. Material parameter values in Mooney-Rivlin models were also adjusted during the cardiac cycle to match Echo volume data. Effective Young's moduli (YM) were calculated for ventricle materials for easy comparison.

Using the mean values of the 1G models as the baseline values, at begin-filling, the mean YM value for the fiber direction (YM_f) from the 2G model was 107% higher than that from the 1G model (723.57 kPa vs. 348.71 kPa). At begin-ejection, YM_f from 2G model was 47% lower than that from the 1G model (85.48 kPa vs. 162.77kPa). According to the total average values, begin-ejection stress and strain from the 2G model were 30% and 14.5% higher than that from the 1G model, respectively (345.16 kPa vs. 265.62 kPa; and 1.0489 vs. 0.9161). Begin-filling stress and strain from the 2G model were 11.5% and 55% higher than that from the 1G model, respectively (2.2613 kPa vs. 2.5543 kPa; and 0.0489 vs.0.1085). During a cardiac cycle, the 2G model begin-ejection YM_f, stress and strain were 19%, 495% and 29% higher than their end-filling value, end-ejection YM_f, stress and strain were 49%, 605% and 297% higher than their begin-filling value, respectively.

The 2G model took ventricle zero-load geometry difference between systole and diastole phases into consideration. This may lead to more accurate ventricle stress/strain calculations and material parameter value estimations.

Keywords: Ventricle modeling; active contraction; ventricle mechanics; Material properties.

Introduction

Myocardial contractility plays a central role in the cardiovascular circulatory system. A non-invasive method for estimating myocardial contractility would be a beneficial tool for cardiologists. As a first-order approximation, an approach using two zero-load geometries (2G) is proposed to model ventricle cardiac motion: one zero-load ventricle geometry is used to model the diastole phase where sarcomere has its relaxed zero-stress length, another zero-load ventricle

geometry is used to model the systole phase where sarcomere has its contracted zero-stress length (therefore the zero-load systole geometry is smaller than the zero-load diastole geometry). Essentially, we are using two models to model the cardiac cycle to handle the active contraction and relaxation which are caused by zero-stress sarcomere length changes.

Active contraction is caused by sarcomere shortening which leads to increased strain and stress (called active strain and stress). At the beginning of active contraction, the zero-stress sarcomere length is shortened in a very short time duration while ventricle volume has no change, so in vivo sarcomere length does not change, which leads to ventricle strain and stress increases, equivalent to the active tension in models in [4][8] for the stress part. McCulloch and Pfeiffer have made great contributions to passive and active ventricle modeling, such as the Physiome Project and the Continuity package [5][9][11]. Guccione et al. proposed the constitutive relations for active stress in cardiac muscle and developed three active tension models [2]-[3]. Liu et al. developed a dynamic cardiac elastography framework to assess the anisotropic viscoelastic passive properties and active contractility of myocardial tissues [6]. Pezzuto and Ambrosi focus on the contraction of the left ventricle in a finite elasticity framework, adopting the “prolate ellipsoid” geometry and the invariants-based strain energy proposed by Holzapfel and Ogden [10]. Our group introduced patient-specific cardiac magnetic resonance (CMR)-based right ventricle/left ventricle models with fluid-structure interactions with various surgical design and potential applications [12]-[15].

In this paper, a new modeling approach using different systole and diastole zero-load geometries was introduced to properly model active contraction and relaxation and obtain ventricle diastole and systole material parameter values, stress and strain conditions. New models were constructed for 10 patients and results were compared with our previously published one-geometry models [7].

Methods

Modeling active contraction and expansion by using different zero-load diastole and systole geometries

Since active LV contraction and relaxation are very complex and involve change of sarcomere zero-stress length which is hard to model using a single no-load LV geometry, some model simplifications are needed to obtain proper models to serve our purposes. Actual LV contraction and expansion involve two different RV zero-stress geometries (diastole and systole) and interconnected changes of LV volume, pressure, stress/strain, and imposed active stress or active material properties. It is commonly accepted that a cardiac cycle may be divided into 4 phases, 2 in diastole (isovolumic relaxation followed by diastolic filling) and 2 in systole (isovolumic contraction followed by systolic emptying). To correctly model these 4 phases, two zero-stress geometries are needed. However, such two-geometry active contraction/expansion models are computationally expensive to construct. McCulloch et al. have introduced active tension in their sophisticated multiscale ventricle models with good success [2]-[3][5]. Tang et al. introduced LV/RV models with fluid-structure interactions using material stiffness variations to handle active contraction and relaxation [13]. Both active tension and stiffness variation approaches involved adding additional terms in tissue material strain energy functions.

Phase 1. Filling (diastole phase). The left ventricle starts with its minimum volume under minimum pressure with minimum stress and strain. One zero-load geometry (diastole geometry) is used for this phase, corresponding to diastole zero-stress sarcomere length (SL). It should be

noted that zero-stress status is a concept for stress/strain calculations. It is not observable in a living heart under in vivo conditions. At beginning-of-filling, mitral valve opens; LV volume increases, pressure increases, in vivo SL expands; strain and stress increases. Phase 1 ends when LV reaches its maximum volume under end-diastole pressure (denoted by P_{dia}) which is lower than the maximum pressure condition.

Phase 2. Isovolumic contraction: Both mitral (inlet) and aortic (outlet) valves are closed; LV volume has no change; zero-stress SL shortens (changing from diastole zero-stress length to systole zero-stress length); however, this sarcomere shortening is not physically observable. Roughly, average in vivo SL does not change much (small local SL changes are possible) since LV volume does not change. So zero-stress SL shortening leads strain and stress increase (This is similar to the active tension in other models, but our model have both strain and stress increase); increased stress pushes pressure to maximum. This phase is short. This phase involves dynamic change of zero-stress sarcomere length which is very difficult to implement. It was skipped in our model.

Phase 3. Ejection (systole phase): This phase starts from max volume, pressure, stress and strain. One zero-load geometry (for systole phase) is used for this phase, corresponding to systole zero-stress SL. At begin-ejection, aortic valve opens up and ejection starts; LV volume drops; in vivo SL shortens and strain decreases; pressure drops; stress drops. At end-systole (end-ejection), LV volume reaches its minimum, pressure drops to the end-systole pressure denoted as P_{sys} , which is greater than minimum pressure. Pressure will continue to drop in Phase 4 when systole zero-stress SL changes to diastole zero-stress SL.

Phase 4. Isovolumic relaxation: Aortic valve closes (both valves closed); zero-stress SL relaxes from systole zero-stress length to diastole zero-stress length (non-contracted length); similar to the comments made in Phase 2, roughly, average in vivo SL does not change much since volume does not change; zero-stress SL relaxation leads to strain and stress decreases; pressure drops to minimum. This phase is short. It was also skipped in our model.

3D echo data acquisition

Patients were recruited to participate in this study with consent obtained (n=10, 7 males, mean age 54.9 years). Echo data acquisitions were performed at the First Affiliated Hospital of Nanjing Medical University, Nanjing, China. Standard echocardiograms were obtained using an ultrasound machine (E9, GE Mechanical Systems, Milwaukee, Wisconsin) with a 3V probe. Patients were examined in the left lateral decubitus position, and images were acquired at end expiration in order to minimize global cardiac movement. Details of the data acquisition procedures were previously described and are omitted here [7]. Figure 1 shows the echo images, zero-load and re-constructed 3D LV geometries.

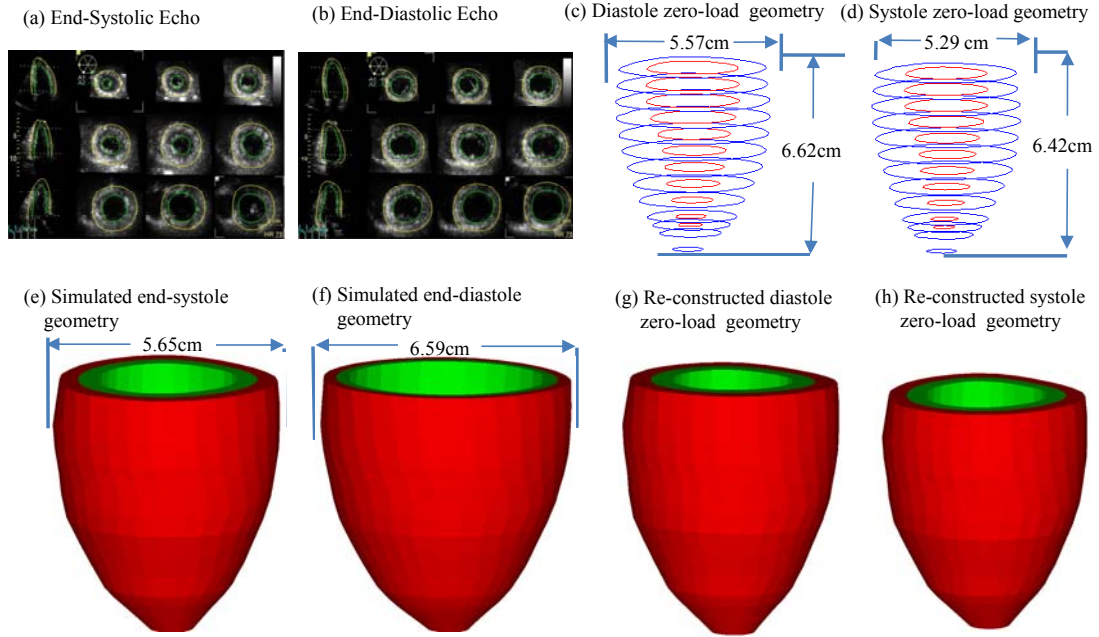


Figure 1. Echo image of a healthy volunteer, contours, zero-load diastole and systole geometries and re-constructed pressurized geometries.

Two-layer anisotropic LV model construction with fiber orientations

Standard governing equations and boundary conditions for the LV model were given:

$$\rho v_{i,tt} = \sigma_{i,j,j}, \quad i, j = 1, 2, 3; \text{ sum over } j, \quad (1)$$

$$\varepsilon_{ij} = (v_{i,j} + v_{j,i} + v_{\alpha,i} v_{\alpha,j}) / 2, \quad i, j, \alpha = 1, 2, 3, \quad (2)$$

where σ is the stress tensor, ε is the strain tensor, v is displacement, and ρ is material density. The normal stress was assumed to be zero on the outer (epicardial) LV surface and equal to the pressure conditions imposed on the inner (endocardial) LV surfaces.

The ventricle material was assumed to be hyperelastic, anisotropic, nearly-incompressible and homogeneous. The nonlinear Mooney-Rivlin model was used to describe the nonlinear anisotropic material properties. The strain energy function for the anisotropic modified Mooney-Rivlin model is given:

$$W = c_1(I_1 - 3) + c_2(I_2 - 3) + D_1[\exp(D_2(I_1 - 3)) - 1] + K_1 / (2K_2) \exp[K_2(I_4 - 1)^2 - 1], \quad (3)$$

where I_1 and I_2 are the first and second strain invariants given by,

$$I_1 = \sum C_{ii}, \quad I_2 = \frac{1}{2}[I_1^2 - \sum C_{ij}C_{ij}], \quad I_4 = \sum C_{ij}(\mathbf{n}_f)_i(\mathbf{n}_f)_j \quad (4)$$

$C = [C_{ij}] = X^T X$ is the right Cauchy-Green deformation tensor, $X = [X_{ij}] = [\partial x_i / \partial a_j]$, (x_i) is the current position, (a_i) is the original position, \mathbf{n}_f is the fiber direction, c_i , D_i and K_i are material parameters chosen to match experimental measurements [1][13]. With parameters properly chosen, it was shown that stress-strain curves derived from Eq. (3) agreed very well with the stress-strain curves from the anisotropic (transversely isotropic) strain-energy function with respect to the local fiber direction given in McCulloch et al.[8]:

$$W = \frac{C}{2}(e^C - 1), \quad (5)$$

$$Q=b_1E_{ff}^2+b_2(E_{cc}^2+E_{rr}^2+E_{cr}^2+E_{rc}^2)+b_3(E_{fc}^2+E_{cf}^2+E_{fr}^2+E_{rf}^2), \quad (6)$$

where E_{ff} is fiber strain, E_{cc} is cross-fiber in-plane strain, E_{rr} is radial strain, and E_{cr} , E_{fr} and E_{fc} are the shear components in their respective coordinate planes, C , b_1 , b_2 , and b_3 are parameters to be chosen to fit experimental data. For simplicity, we set $b_1=0.8552$, $b_2=1.7005$, $b_3=0.7742$ in Eq. (6) so that we can have a single parameter C for comparison. The least-squares method was used to find the equivalent Young's moduli (YM) for the material curves for easy comparison. Active contraction and expansion of myocardium were modeled by material stiffening and softening in our model. Material stiffening and softening were achieved by adjusting parameter values at each Echo-time step (28 Echo frames per cycle) to simulate active contraction and expansion and match LV volume data.

As patient-specific fiber orientation data was not available from these patients, we chose to construct a two-layer LV model and set fiber orientation angles using fiber angles given in Axel [1]. Fiber orientation angles were set at -60 degree and 80 degree for epicardium (outer layer) and endocardium (inner layer), respectively. Fiber orientation can be adjusted when patient-specific data becomes available [12].

A pre-shrink process and geometry-fitting technique for mesh generation

Under in vivo condition, ventricles were pressurized and the no-load ventricular geometries were unknown. In our model construction process, an iterative pre-shrink process was applied to the in vivo minimum volume ventricular geometry to obtain the two zero-load geometries so that when in vivo pressure was applied, the ventricle would regain its in vivo geometry. To get the zero-load diastole geometry, we start with a 4% shrinkage, construct the model, and apply the minimum pressure to see if the pressurized LV volume matches the Echo data. If not, we adjust the shrinkage, re-made the model, pressurize it and check again. The process is repeated until LV volume matches Echo volume with error < 0.5%. For the zero-load systole geometry, assuming a 10-15% sarcomere shortening, we start with a 14% shrinkage. Different shrinkage rates were used for LV inner and outer surfaces so that mass conservation law was enforced. The same process was repeated until the pressurized LV volume under end-systole pressure matched the Echo-measured end-systole volume data.

A geometry-fitting mesh generation technique was also used to generate mesh for our models [13]. Mesh analysis was performed by decreasing mesh size by 10% (in each dimension) until solution differences were less than 2%. The mesh was then chosen for our simulations.

Solution methods and Data collection for Statistical analysis

The anisotropic LV computational models were constructed for ten patients and the models were solved by ADINA (ADINA R&D, Watertown, MA, USA) using unstructured finite elements and the Newton-Raphson iteration method. Stress/strain distributions were obtained for analysis. Because stress and strain are tensors, for simplicity, maximum principal stress (Stress-P₁) and strain (Strain-P₁) were used and referred to as stress and strain in this paper. For each LV data set (11 slices. Slices are short-axis cross sections), we divided each slice into 4 quarters, each quarter with equal inner wall circumferential length. Ventricle wall thickness, circumferential curvature (C-curvature), longitudinal curvature (L-curvature) and stress/strain were calculated at all nodal points (100 points/slice, 25 points/quarter). The “quarter” values of those parameters were obtained by taking averages of those quantities over the 25 points for each quarter and

saved for analysis. The quarter values of those from the ten patients were compared to see if there are any statistically significant differences.

Results and Discussion

The purpose of this paper is to introduce the new model with 2 zero-load geometries (2G model), compare the results with our previous model which used 1 zero-load geometry (1G model). For the 1G model, results at begin-filling (BF) and begin-ejection (BE) corresponding to minimum and maximum pressure and LV volume were obtained for comparison. For the 2G model, results at begin-filling (BF), end-filling (EF), begin-ejection (BE), and end-ejection (EE) were obtained for comparison. Due to 1G model limitation, EF and BE from 1G model had the same geometry, pressure and material conditions. Therefore, 1G EF and BE stress/strain values were also the same.

Human ventricle tissue material properties are extremely hard to quantify noninvasively under in vivo conditions. Myocardium material stiffness changes in a cardiac cycle. Figure 2 gives the stress-stretch curves for 1G and 2G models from one patient to illustrate the material differences. Bar plots of mean YM_f value in the fiber direction (YM_f) of the 10 patients from 1G and 2G models were in Fig. 3 (a) showing clear comparisons. Using the mean values of 1G models as the baseline values, at BF, YM_f from 2G model was 107% stiffer than that from the 1G model (723.57 kPa vs. 348.71 kPa). At BE, YM_f from 2G model was 47% lower than that from the 1G model (85.48 kPa vs. 162.77kPa). At EF, YM_f from 2G model was 56% lower than that from the 1G model (71.683 kPa vs. 162.77kPa). At EE, YM_f from 2G model was 210% higher than that from the 1G model (1080.95 kPa vs. 348.71 kPa). This indicated the material parameter properties from 2G models were stiffer than that from 1G model at BF and EE corresponding to minimum LV volume, and softer than that from 1G model at BE and EF corresponding to maximum LV volume. From 2G models, BE YM_f was 19% higher than its EF value (85.48 kPa vs. 71.68 kPa), EE YM_f was 49% higher than its BF value (1080.95 kPa vs. 723.57 kPa).

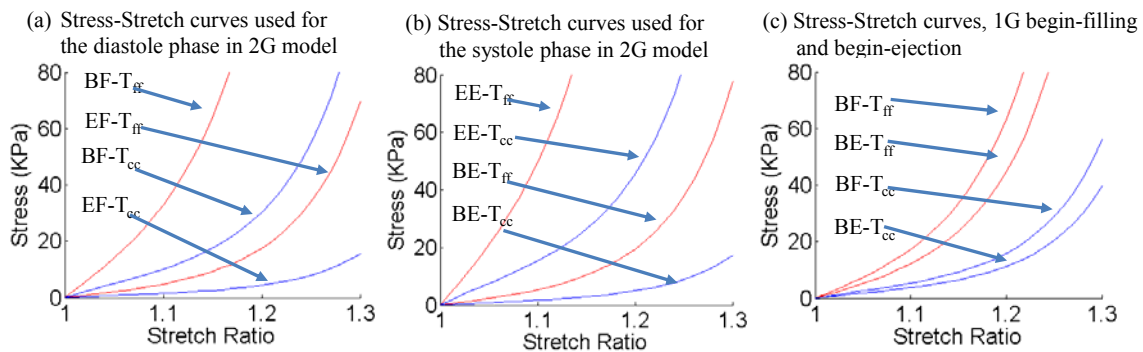


Figure 2. Material Stress-Stretch curves and YM_f comparison for 1G and 2G models. T_{ff} : stress in fiber direction; T_{cc} : stress in circumferential direction. YM_f : Young's Modulus in fiber direction. BF: Begin-Filling; EF: End-Filling. BE: Begin-Ejection; EE: End-Ejection.

Table 1. Material parameters from the 2G and 1G models.

	C(kPa)	Y _{Mf} (kPa)	C(kPa)	Y _{Mf} (kPa)	C(kPa)	Y _{Mf} (kPa)
	1G-BF		2G-BF		2G-EF	
P1	10.102	290.47	18.9420	544.62	2.3813	68.467
P2	11.185	321.59	25.9776	746.91	2.3452	67.429
P3	11.365	326.77	21.6480	622.43	3.1390	90.252
P4	10.283	295.65	19.1224	549.81	2.8503	81.953
P5	11.419	328.33	19.8440	570.56	2.1648	62.243
P6	14.432	414.95	28.8640	829.91	1.7860	51.350
P7	13.530	389.02	31.5700	907.70	1.5695	45.126
P8	10.102	290.47	21.6480	622.43	4.4198	127.08
P9	19.483	560.18	46.9040	1348.59	1.2628	36.308
P10	9.3808	269.72	17.1380	492.75	3.0127	86.621
Mean	12.128	348.71	25.1658	723.57	2.4931	71.683
	1G-BE		2G-BE		2G-EE	
P1	5.7367	164.94	2.4895	71.579	31.029	892.14
P2	5.2857	151.98	2.6519	76.247	38.425	1104.8
P3	8.0278	230.82	3.4998	100.625	32.652	938.82
P4	7.7211	102.23	3.7523	107.887	31.390	902.52
P5	6.0073	172.72	2.3272	66.911	33.735	969.95
P6	4.5100	129.67	2.0205	58.093	38.786	1115.2
P7	3.6621	105.29	1.8040	51.869	45.100	1296.7
P8	9.4710	272.31	6.4944	186.728	37.884	1089.2
P9	2.9586	85.065	1.3710	39.420	52.316	1504.2
P10	7.3964	212.66	3.3194	95.439	34.637	995.88
Mean	6.0777	162.77	2.9730	85.480	37.595	1080.95

Table 2 summarizes the average stress and strain values of the 10 patients from the 1G and 2G models. Bar plots of mean stress/strain values of the 10 patients from 1G and 2G models were in Fig. 3 (b) and (c) showing clear comparisons. According to the total average values in Table 3, BE stress values from the 2G model was 30% higher than that from the 1G model (345.16 kPa vs. 265.62 kPa). BF stress values from the 2G model was 14.5% lower than that from the 1G model (2.2613 kPa vs. 2.5543 kPa). BE strain values from the 2G model was 11.5% higher than that from the 1G model (1.0489 vs. 0.9161). BF strain values from the 2G model was 55% lower than that from the 1G model (0.0489 vs. 0.1085). From 2G models, BE stress average value was 511% higher than its EF value (354.16 kPa vs. 57.96 kPa), EE stress average value was 605% higher than its BF value (15.94 kPa vs. 2.26 kPa). BE strain average value was 29% higher than its EF value (1.0489 vs. 0.8110), EE strain average value was 297% higher than its BF value (0.1942 vs. 0.0489). Bar plots of wall thickness and curvature results in Fig. 3 (d)-(f) shows the geometrical characteristics from the 1G and 2G models were about the same.

Table 2. Comparison of average stress and strain results from 2G and 1G models

Patient	1G-BF	1G-BE	2G-BF	2G-EF	2G-BE	2G-EE
Average stress						
P1	2.3290	224.68	1.9345	47.986	311.31	15.429
P2	2.8488	293.62	2.6241	58.033	372.43	17.785
P3	2.3849	185.83	2.0071	37.989	265.97	15.331
P4	2.4531	186.16	1.8084	30.841	255.31	14.907
P5	2.5214	290.74	2.3700	62.283	401.50	16.690
P6	2.2008	277.08	2.0724	64.571	353.67	13.015
P7	1.8442	292.55	1.7388	74.045	363.51	12.619
P8	3.4650	221.26	2.8673	41.191	261.86	18.875
P9	2.7979	408.15	2.6838	105.48	495.94	15.139
P10	2.6982	276.19	2.5062	57.221	370.09	19.644
Mean	2.5543	265.62	2.2613	57.964	345.16	15.943
Average strain						
P1	0.1121	0.8845	0.0508	0.7820	1.0297	0.2120
P2	0.1228	0.9206	0.0502	0.7972	1.0360	0.2021
P3	0.1103	0.8492	0.0497	0.7437	1.0135	0.2172
P4	0.1215	0.8438	0.0496	0.7150	0.9860	0.2145
P5	0.1110	0.9293	0.0613	0.8437	1.0948	0.2185
P6	0.0826	0.9910	0.0393	0.9049	1.1325	0.1700
P7	0.0716	0.9935	0.0291	0.9102	1.1110	0.1403
P8	0.1514	0.8061	0.0615	0.6632	0.8768	0.2042
P9	0.0726	1.0780	0.0289	0.9904	1.2036	0.1403
P10	0.1292	0.8654	0.0684	0.7598	1.0053	0.2227
Mean	0.1085	0.9161	0.0489	0.8110	1.0489	0.1942

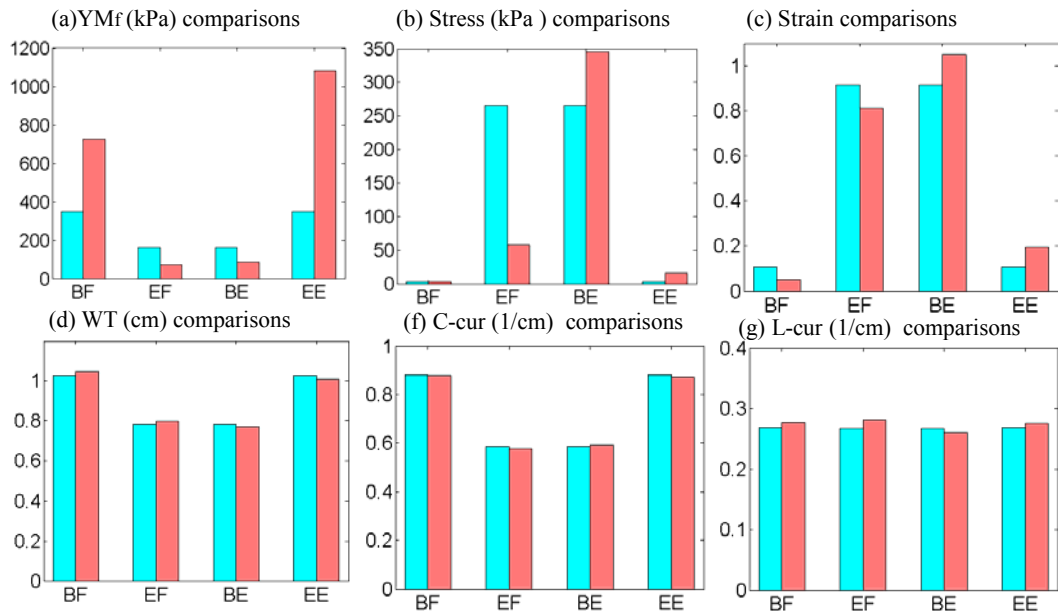


Figure 3. Bar plots for LV Y_{Mf} , Stress, Strain, wall thickness (WT), circumferential curvatures (C-cur) , longitudinal curvature (L-cur) comparisons from 1G and 2G models. Blue: 1G; Red: 2G.

Conclusions

Correct stress/strain calculation is of fundamental importance for many cardiovascular research where mechanical forces play a role. Ventricle remodeling, disease development, tissue regeneration, patient recovery after surgery and many other cell activities are closely associated with ventricle mechanical conditions. The 2G modeling approach is setting up the right stage for diastole and systole stress/strain calculations using proper zero-load geometries. 1G models do not use different reference geometries for systole and diastole phases, therefore have difficulties in giving right strain calculations. It should be noted that direct measurements of stress, strain, and zero-load sarcomere length are either extremely difficult or even impossible. Even by using tagging, the strain determined uses in vivo references and could not account for zero-stress SL changes. Actual ventricle contraction and relaxation are very complex. Our model is only a first-order approximation, an improvement over the 1G models. Lack of in vivo data and model construction cost are also considerations. Data from the literature or from ex vivo experiments have to be used to complete the computational models. We are in need of patient-specific data such as fiber orientation, sarcomere length contraction rate, regional material properties, etc.

Acknowledgement. This research was supported in part by National Sciences Foundation of China grants 11672001, 81571691. Longling Fan's research is supported in part by the Fundamental Research Funds for the Central Universities (KYLX15_0110) and the Scientific Research Foundation of Graduate School of Southeast University (YBJJ1617).

References

- [1] Axel, L. (2002) Biomechanical dynamics of the heart with MRI, *Annu. Rev. Biomed. Eng.* **4**, 321-347.
- [2] Guccione, J. M. and McCulloch, A. D. (1993a) Mechanics of active contraction in cardiac muscle: Part I—Constitutive relations for fiber stress that describe deactivation, *J. Biomech. Eng.* **115**, 72–81.
- [3] Guccione, J. M., Waldman, L. K. and McCulloch, A. D. (1993) Mechanics of active contraction in cardiac muscle: Part II—Cylindrical models of the systolic left ventricle, *J. Biomech. Eng.* **115**, 82–90.
- [4] Hunter, P. J., Pullan, A. J., Smaill, B. H. (2003) Modeling total heart function. *Annu Rev Biomed Eng.* **5**, 147-77.
- [5] Kerckhoffs, R. C. P., Healy, S. N., Usyk, T. P. and McCulloch, A. D. (2006) Computational methods for modeling cardiomechanics, *Proc IEEE.* **94**, 769-783.
- [6] Liu, Y., Wang, G. and Sun, L. Z. (2006) Anisotropic elastography for local passive properties and active contractility of myocardium from dynamic heart imaging sequence, *Int J Biomed Imaging.* **2006**, 45957.
- [7] Fan, L. L., Yao, J., Yang, C., Tang, D. and Xu, D. (2015) Infarcted Left Ventricles Have Stiffer Material Properties and Lower Stiffness Variation: 3D Echo-Based Modeling to Quantify In Vivo Ventricle Material Properties, *J. Biomech. Eng.* **137**, 081005.
- [8] McCulloch, A. D., Waldman, L., Rogers, J. and Guccione, J. M. (1992) Large-scale finite element analysis of the beating heart, *Critical Rev. in Biomed. Eng.* **20**, 427-449.
- [9] McCulloch, A. D., et al. (2007) Continuity 6, www.continuity.ucsd.edu.
- [10] Pezzuto, S. and Ambrosi, D. (2014) Active contraction of the cardiac ventricle and distortion of the microstructural architecture, *Int J Numer Method Biomed Eng.* **30**, 1578-1596.
- [11] Pfeiffer, E., Tangney, J. R., Omens, J. H. and McCulloch, A. D. (2014) Biomechanics of cardiac electromechanical coupling and mechanoelectric feedback, *J. Biomech. Eng.* **6**, 021007.
- [12] Tang, D., Yang, C., Geva, T. and del Nido, P. J. (2008) Patient-specific MRI-based 3D FSI RV/LV/Patch models for pulmonary valve replacement surgery and patch optimization, *J. of Biomech. Eng.* **130**, 041010.
- [13] Tang, D., Yang, C., Geva, T. and del Nido, P. J. (2010) Image-Based Patient-Specific Ventricle Models with Fluid-Structure Interaction for Cardiac Function Assessment and Surgical Design Optimization, *Progress in Pediatric Cardiology* **30**, 51-62.
- [14] Tang, D., Yang, C., Geva, T., Gaudette, G. and del Nido, P. J. (2011) Multi-physics MRI-based two-layer fluid-structure interaction anisotropic models of human right and left ventricles with different patch materials: cardiac function assessment and mechanical stress analysis, *Computers & Structures* **89**, 1059-1068.
- [15] Tang, D., del Nido, P. J., Yang, C., Zuo, H., Huang, X. Y., Rathod, R. H., Tang, A., Wu, Z. Y., Billiar, K. L. and Geva, T. (2016) Patient-Specific MRI-Based Right Ventricle Models Using Different Zero-Load Diastole and Systole Geometries for Better Cardiac Stress and Strain Calculations and Pulmonary Valve Replacement Surgical Outcome Predictions, *PLOS One* **11**, e0162986.